Supporting Information

Tian et al. 10.1073/pnas.1017762108

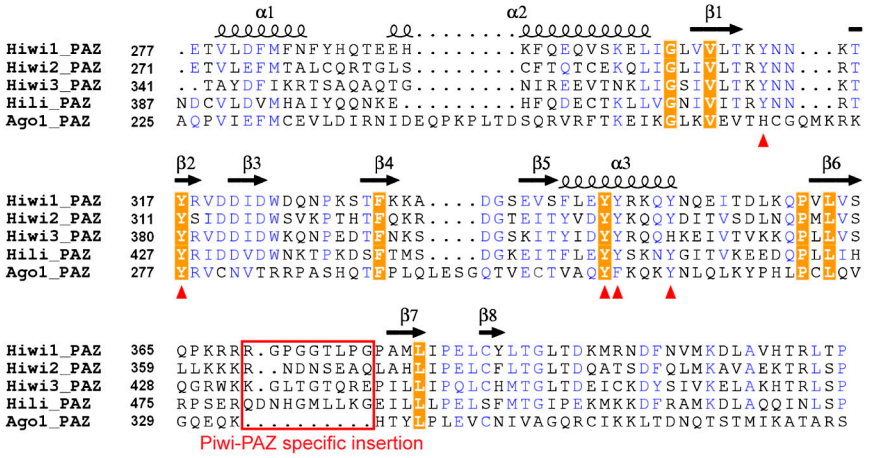

Fig. S1. Sequence alignment of human Piwi and Ago PAZ (Piwi/Argonaute/Zwille) domains. Amino acid sequence alignment of PAZ domains from human Piwi family members Hiwi1, Hiwi2, Hiwi3, Hili, and human Ago1. A red box highlights the Piwi PAZ-specific insertion element between strands β6 and β7. Conserved side chains are shown in an orange background, whereas those lining the binding pocket for the 2-nt segment at the 3′ end are indicated by red triangles.

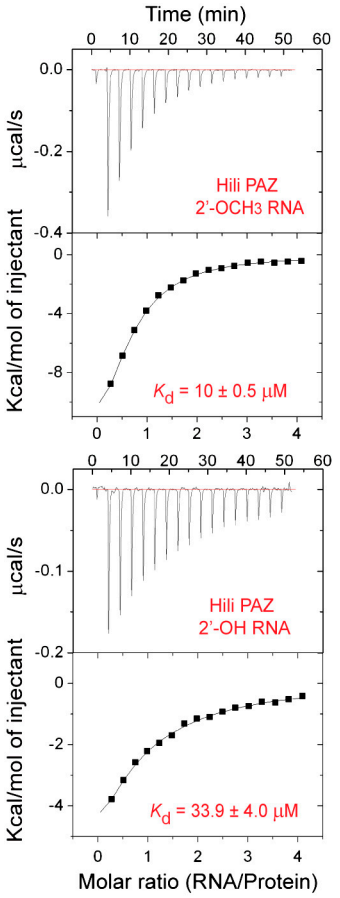

Fig. S2. RNA binding analysis on Hili PAZ domain. Isothermal titration calorimetry measurements for binding of Hili PAZ to self-complementary 14-mer RNA containing 2′-OCH_3 (*Upper*) and 2′-OH (*Lower*) at the 3′ end.

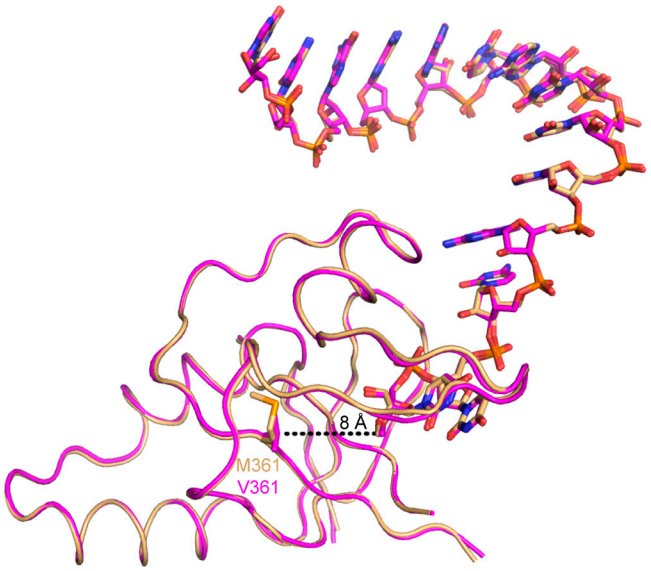

Fig. S3. Structural superposition of RNA bound complexes of wild-type and V361M mutant Hiwi1 PAZ domains. Wild-type Hiwi1 and V361M PAZ domains are colored in magenta and biscuit. The side chains of Val361 in wild-type and Met361 in V361M mutant Hiwi1 PAZ are shown in stick representation. The dotted line shows the distance between the methyl group of Um14 and Val361/Met361 of PAZ domain.

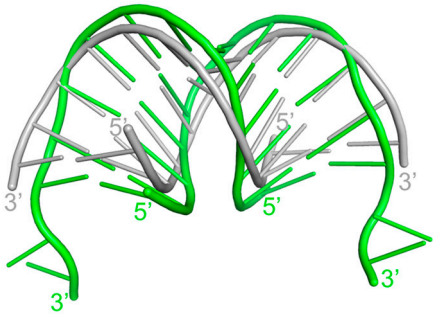

Fig. S4. Structural superposition and comparison of double-stranded RNA (dsRNA) observed in Hiwi1 PAZ-RNA complex and ideal A-form helix. The dsRNA in the Hiwi PAZ complex is colored green, whereas the ideal A-form dsRNA is colored in silver.

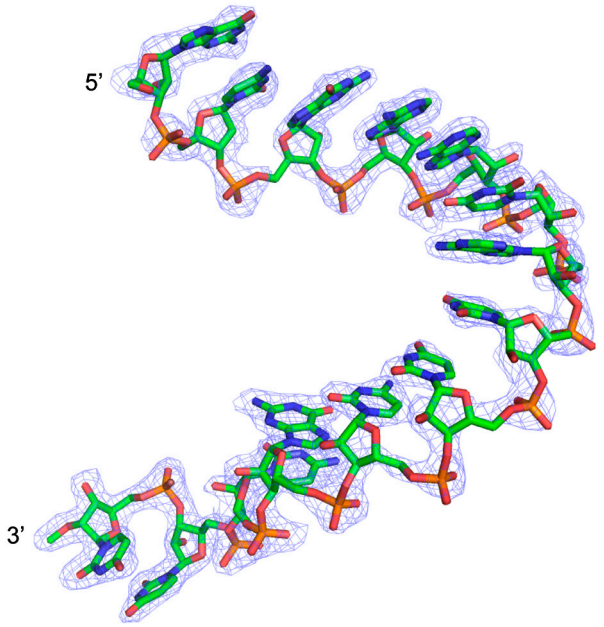

Fig. S5. Electron density for the RNA strand in Hiwi1 PAZ-RNA complex. The $2F_o - F_c$ map (contoured at 1.2σ) corresponding to one strand of the RNA present in the asymmetric unit.

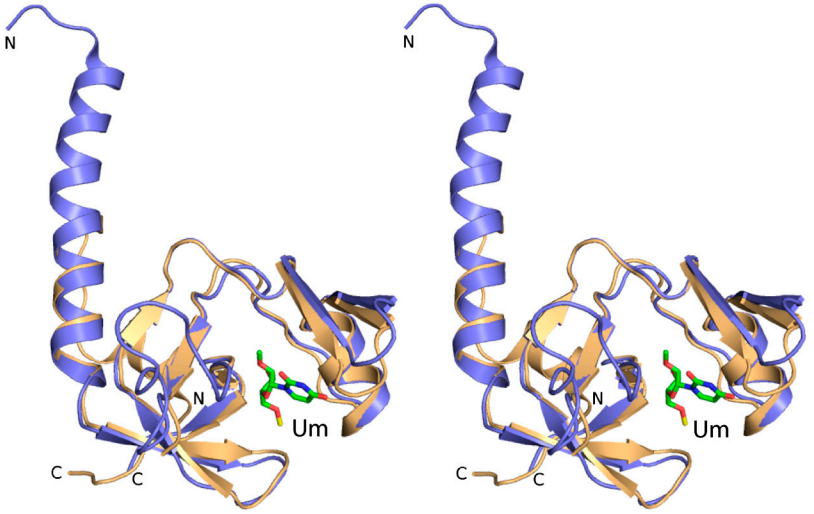

Fig. S6. Structural superposition in stereo of Hili PAZ in the free state and Hiwi1 PAZ in their RNA bound states. Comparison of Hili PAZ domain (in blue) and Hiwi1 PAZ domain (in biscuit) with bound 2′-Um (Um stands for the 3′-terminal U modified by a 2′-OCH_3 group) at 3′ end (in green)

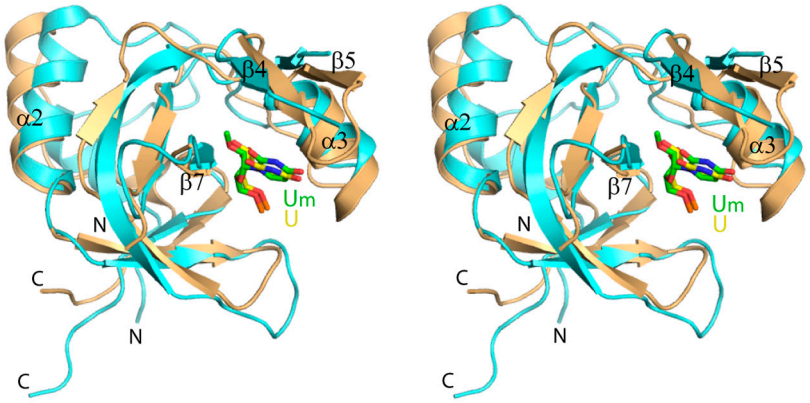

Fig. S7. Structural superposition in stereo of Hiwi1 PAZ and Ago1 PAZ in their RNA bound states. Comparison of Hiwi1 PAZ domain (in biscuit) with bound 2′-Um at 3′ end (in green) and Ago1 PAZ (in cyan) with bound 2′-U at 3′ end (in yellow).

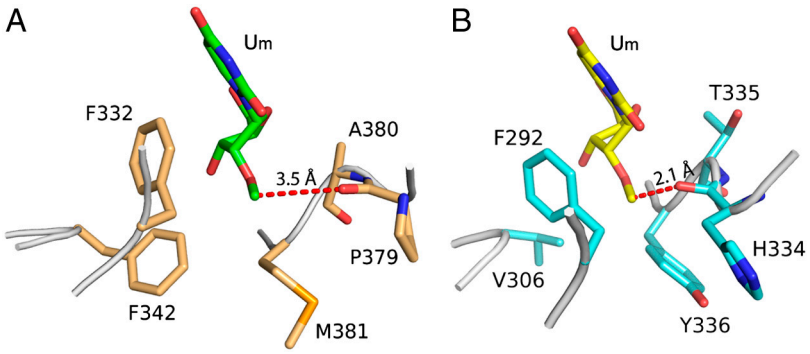

Fig. S8. Steric constraints following insertion of a 2′-OCH_3 group at the RNA 3′ end into the Ago1 PAZ but not Hiwi1 PAZ-binding pocket. (*A*) Insertion of the 2′-OCH_3 group at the 3′ end of bound RNA into the PAZ-binding pocket of the Hiwi1 PAZ-RNA complex. The separation between methyl carbon of the 2′-OCH_3 group and a backbone carbonyl is ≈3.5 Å. (*B*) Insertion of the 2′-OCH_3 group (model based on position of 2′-OH group) at the 3′ end of bound RNA into the PAZ-binding pocket of the Ago1 PAZ-RNA complex. The separation between methyl carbon of the modeled 2′-OCH_3 group and a backbone carbonyl is ≈2.1 Å, indicative of a steric clash.

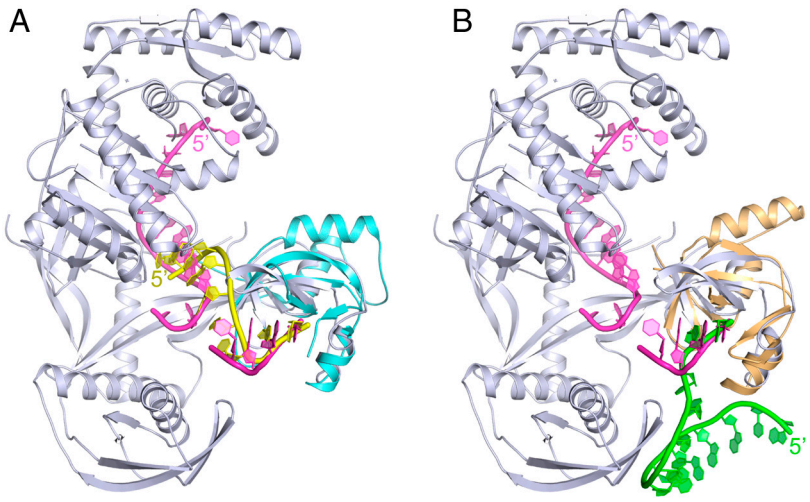

Fig. S9. Comparison of overhang-strand containing trajectories observed in the structures of human Ago1 PAZ-RNA complex [Protein Data Bank (PDB) ID 1SI3] and human Hiwi1 PAZ-RNA complex with respect to guide strand orientation in *Thermus thermophilus* Ago (PDB ID 3DLH). Structural superposition of guide strand (colored in magenta) containing *Thermus thermophilus* Ago (colored in light blue) with (*A*) human Ago1 (colored in cyan) in complex with RNA (colored in yellow) and (*B*) human Hiwi1 PAZ (colored in wheat) in complex with RNA (colored in green).

Table S1. Crystallographic data collection and refinement statistics

	Hiwi1(V361M) PAZ-RNA complex 2′-OCH_3 at 3′ end	Hiwi1 PAZ-RNA complex 2′-OCH_3 at 3′ end	Hiwi1 PAZ-RNA complex 2′-OH at 3′ end	Hili PAZ
Data collection				
Wavelength, Å	0.9792	0.9792	0.9792	0.9792
Space group	$P4_122$	$P4_122$	$P4_122$	$C222_1$
Unit cell				
a, *b*, *c*, Å	44.45, 44.5, 147.2	44.0, 44.0, 147.0	44.3, 44.3, 147.7	40.5, 142.9, 226.5
α, β, γ, °	90, 90, 90	90, 90, 90	90, 90, 90	90, 90, 90
Resolution, Å	20.0-2.1 (2.17-2.10)	30.0-2.9 (3.0-2.9)	20.0-2.8 (2.9-2.8)	50.0-2.92 (3.02-2.92)
Total reflections	316,709	190,815	130,613	214,388
Unique reflections	9,323	3,631	4,130	14,822
$I/\sigma I$	38.4 (15.0)	32.5 (4.8)	14.8 (1.9)	20.2 (3.0)
Completeness, %	99.4 (100.0)	95.3 (72.3)	96.6 (78.7)	95.1 (67.2)
Redundancy	11.4 (12.0)	10.4 (6.2)	4.1 (2.8)	6.9 (4.7)
R_{merge}	5.9 (18.0)	8.3 (20.9)	9.6 (36.1)	9.1 (30.7)
Refinement				
R_{work}/R_{free}	23.5/27.9	25.2/30.5	24.3/29.7	24.6/29.3
No. of atoms				
Protein	874	855	871	3,578
RNA	293	293	292	0
Water	52	6	22	9
Average B factors, $Å^2$				
Protein	35.6	60.2	45.5	75.3
RNA	44.3	65.8	48.9	—
Water	44.8	38.9	38.4	61.4
rmsd				
Bond lengths, Å	0.010	0.005	0.005	0.005
Bond angles, °	1.383	0.842	0.849	0.887
Ramachandran statistics, %				
Mostly allowed regions	94.3	94.4	94.8	82.9
Allowed regions	5.7	5.6	5.2	14.3
Generously allowed regions	0.0	0.0	0.0	2.6
Disallowed regions	0.0	0.0	0.0	0.3

Values in parentheses are for highest-resolution shell. $R_{work} = \Sigma|F_o\text{-}F_c|/\Sigma F_o$. R_{free} is the cross-validation of *R* factor.